

# Exact low-dimensional description for fast neural oscillations with low firing rates

Pau Clusella<sup>1,\*</sup> and Ernest Montbrió<sup>2</sup>

<sup>1</sup>*Departament de Matemàtiques, Universitat Politècnica de Catalunya, 08242 Manresa, Spain*

<sup>2</sup>*Neuronal Dynamics Group, Department of Information and Communication Technologies, Universitat Pompeu Fabra, 08018 Barcelona, Spain.*

Recently, low-dimensional models of neuronal activity have been exactly derived for large networks of deterministic, Quadratic Integrate-and-Fire (QIF) neurons. Such *firing rate models* (FRM) describe the emergence of fast collective oscillations ( $>30$  Hz) via the frequency-locking of a subset of neurons to the global oscillation frequency. However, the suitability of such models to describe realistic neuronal states is seriously challenged by fact that during episodes of fast collective oscillations, neuronal discharges are often very irregular and have low firing rates compared to the global oscillation frequency. Here we extend the theory to derive exact FRM for QIF neurons to include noise, and show that networks of stochastic neurons displaying irregular discharges at low firing rates during episodes of fast oscillations, are governed by exactly the same evolution equations as deterministic networks. Our results reconcile two traditionally confronted views on neuronal synchronization, and upgrade the applicability of exact FRM to describe a broad range of biologically realistic neuronal states.

## I. INTRODUCTION

Fast oscillations ( $>30$  Hz) are a prominent feature of neural activity [1–4]. Empirical studies show that very often such rhythms display a remarkable dichotomy: At the collective level, neuronal oscillations are fast and fairly regular, whereas at the single-cell level individual spikes trains remain highly irregular and have low firing rates [4–6].

A wealth of theoretical and computational work have investigated the emergence of fast neuronal rhythms, and identified minimal neurophysiological ingredients that robustly produce them in large ensembles of spiking model neurons [2–7]. According to these studies, fast oscillations emerge in populations of inhibitory neurons with synaptic time constants and/or fixed delays, and sufficient drive to induce spiking. Notably, in this idealized modeling framework of neuronal synchrony, networks of spiking neurons with random connectivity and additive noise may display irregular spike discharges at low firing rates, akin to experimental observations [8, 9]. This so-called *sparse synchronization* [6] state, is also encountered in all-to-all coupled networks with both multiplicative and additive noise [8, 9], or just with additive noise [10, 11].

An alternative and powerful tool to investigate fast neuronal oscillations is to use reduced or simplified models —called neural-mass, or firing-rate models (FRM)—, which describe the mean activity in a neuronal population [12–15]. Such FRM consist of one, or a few ordinary differential equations, and allow for a thorough understanding of the system’s dynamics. Specifically, for the case of an inhibitory network with synaptic delays, FRM exhibit fast oscillations similar to those observed in numerical simulations of large networks of spiking neurons [16–19].

Fast oscillations in FRM are often associated to the presence of sparse synchronization [6, 20]. However, the fact that FRM are heuristic and not exactly obtained from a given network of spiking neurons, impedes one from unambiguously linking the collective dynamics described by the FRM with

that of individual neurons in the network. Yet, a notable exception is a recently developed mean-field theory that allows for a proper mathematical derivation of the FRM corresponding to an all-to-all coupled ensemble of heterogeneous, Quadratic Integrate-and-Fire (QIF) neurons [21, 22]. Accordingly, this theory is singularly suited to investigate the relation between microscopic, single-cell dynamics (observed in numerical simulations of networks of spiking neurons), with that of the network’s collective states —exactly described by the QIF-FRM.

Unfortunately, the theory to obtain QIF-FRM (also known as ‘next-generation neuron mass models’ [23]), is only valid for deterministic networks with Cauchy heterogeneity, which are not capable of displaying sparsely synchronized states. Indeed, synchronization emerging in populations of heterogeneous inhibitory neurons is due to the frequency entrainment of a subset of neurons, which display regular, periodic dynamics with the (fast) frequency of the collective rhythm [10, 18, 19, 23–35]. This synchronization scenario for deterministic neurons is in sharp contrast with the sparse synchronization scenario, and seriously challenges the suitability of QIF-FRM to describe and investigate biologically plausible neuronal states. In addition, synchronization in such heterogeneous networks is considered to be fragile and at odds with sparse synchronization [4–6, 10].

Motivated by recent advances in the context of the Kuramoto model [36, 37], in this article we extend the theory to derive QIF-FRM to networks of QIF neurons driven by Cauchy noise. Strikingly, the resulting QIF-FRM reveals that deterministic QIF networks showing fast oscillations via frequency-entrainment are governed by the same evolution equations as networks of stochastic QIF neurons displaying sparse synchronization.

## II. SYNCHRONIZATION SCENARIOS IN POPULATIONS OF INHIBITORY QIF NEURONS

We consider a population of  $N$  QIF neurons [38, 39], interacting via a mean-field inhibitory coupling of strength  $J$ . The evolution of the membrane potential of a QIF neuron obeys

\* pau.clusella@upc.edu

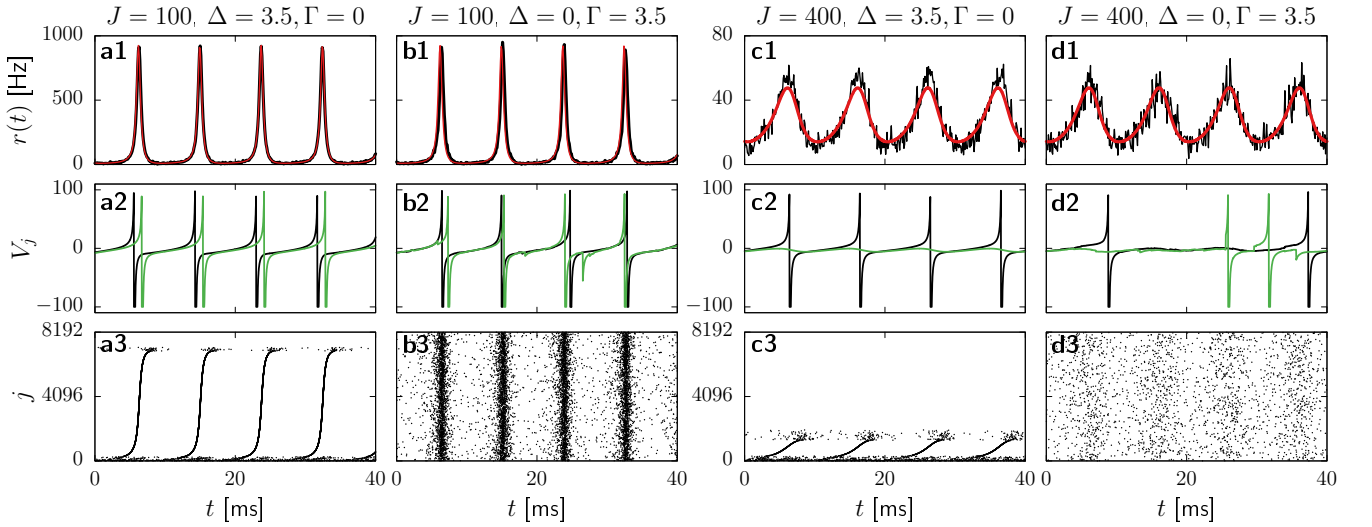


FIG. 1. Synchronization scenarios in an inhibitory network of globally coupled QIF neurons, Eqs. (1,2), with quenched Cauchy heterogeneity (panels (a1)–(a3) and (c1)–(c3)), and with Cauchy noise (panels (b1)–(b3) and (d1)–(d3)), and  $\bar{\eta} = 100$ . Panels (a1)–(d1): Black lines: Time series of the mean firing rate Eqs. (1,2). Red lines: Time series of the  $r$ -variable of the QIF-FRM (12,2). Panels (a2)–(d2): Time series of the membrane potential of two individual QIF neurons. Panels (a3)–(d3): Raster plots of the spiking times of a subset of 25% of randomly selected neurons. Neuron indices in panels (a3) and (c3) are sorted according to  $\eta_j$ .

the equation

$$\tau_m \dot{V}_j = V_j^2 + \eta_j + \xi_j(t) - \tau_m J s(t), \quad (1)$$

where  $j = 1, \dots, N$ , and the following resetting rule: if  $V_j > V_p$  then  $V_j \leftarrow V_r$ . The neuron's membrane time constant  $\tau_m$  is set to 10 ms, and quenched heterogeneity is modeled via parameter  $\eta_j$ , which represents a constant input current that varies from neuron to neuron according to a Cauchy probability density function  $G(\eta)$ , centered at  $\bar{\eta}$  and with half-width at half-maximum (HWHM)  $\Delta$ ,

$$G(\eta) := \frac{1}{\pi} \frac{\Delta}{(\eta - \bar{\eta})^2 + \Delta^2}.$$

In addition, neurons are subject to independent noisy inputs. Specifically, the random variables  $\xi_j(t)$  represent zero-centered Cauchy white noise with HWHM  $\Gamma$ . Finally, neurons interact all-to-all through the mean post-synaptic activity  $s(t)$ . This mean field variable is related via the equation

$$\tau_s \dot{s}(t) = -s(t) + r(t), \quad (2)$$

to the population mean firing rate  $r(t)$

$$r(t) = \frac{1}{N} \sum_{j=1}^N \sum_k \frac{1}{\tau_r} \int_{t-\tau_r}^t d\zeta \delta(\zeta - t_j^{(k)}). \quad (3)$$

The time constant  $\tau_s$  in Eq. (2) corresponds to the synaptic decay time of the inhibitory synapses, which we set to  $\tau_s = 5$  ms. The instant  $t_j^{(k)}$  in Eq.(3) indicates the  $k$ -th spike of neuron  $j$ , and  $\tau_r$  is a time window of the spike events, which we set to  $10^{-2}$  ms [40].

In Figure 1, we compare the results of numerical simulations [41] in two different synchronous regimes of Eqs. (1,2),

using deterministic and noisy networks. For moderated inhibition, the mean firing rate  $r(t)$  displays fast oscillations at approximately 100 Hz, which are noticeably similar in both the deterministic and the noisy network, see Fig. 1(a1) and Fig.1(b1), respectively. The large amplitude of the firing rate oscillations reflects a high degree of synchronization. Indeed, Figs. 1(a2) and 1(b2) show the membrane potential of two neurons in the heterogeneous and noisy networks respectively. In both cases, neurons fire periodically with the frequency of the global oscillations. Additionally, the raster plots in Figs. 1(a3) and 1(b3) confirm that most neurons display such regular, periodic dynamics.

In contrast, for strong inhibitory coupling ( $J = 400$ ), the amplitude of the oscillations is greatly reduced (see Figs. 1(c1,d1), and the striking similarity between the firing rate dynamics of the deterministic and the stochastic networks) and the microscopic states of the two networks strongly differ. Indeed, the raster plot of the deterministic population Fig 1(c3) shows that only a small subset of the neurons fire regularly, while a majority is strongly suppressed due to feedback inhibition [25]. On the other hand, in the stochastic network, noise may release some of the neurons from suppression, producing highly irregular spike trains, with low firing rates and little indication of the collective oscillation, see Figs. 1(d2,d3). This latter state corresponds to the sparse synchronization originally uncovered in networks of inhibitory neurons [8, 9].

To further emphasize the effects of noise in synchronized states, in Fig. 2 (solid lines) we computed the distribution of interspike intervals (ISI) corresponding to the synchronization regimes shown in columns b and d of Fig. 1. Figure 2(a) indicates that, for weak inhibition, the distribution has a large peak that coincides with the collective oscillation

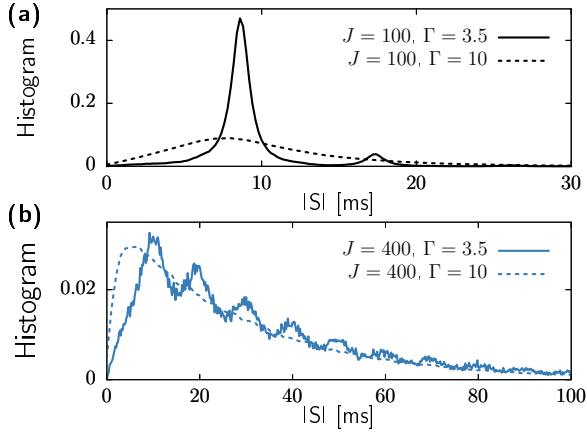


FIG. 2. Interspike interval (ISI) histograms of populations of stochastic QIF neurons for  $J = 100$  (panel a) and  $J = 400$  (panel b). Continuous lines correspond to the results in Fig 1(b3,d3) ( $\Gamma = 3.5$ ), dashed lines correspond to a asynchronous state ( $\Gamma = 10$ ).

period ( $T \approx 8.7\text{ms}$ ). In addition, there is a small resonance in a second harmonic, indicating that most neurons fire once per cycle and, due to noise, some skipping events occur. The corresponding Coefficient of Variation—quantifying the broadness of the ISI distribution—is  $\text{CV} \approx 0.35$ , which confirms that, despite the presence of noise, spike trains remain highly regular [42]. Figure 2(b) shows the ISI histogram for strong inhibition. In this case the distribution is broad ( $\text{CV} = 0.85$ ), spanning several periods of the oscillation cycle, with small peaks located at the harmonics of the fundamental period. This indicates that spike trains are highly irregular, and close to a Poisson process ( $\text{CV} = 1$ ). In asynchronous regimes, the additional peaks of the ISI distribution vanish, leading to a unimodal histogram (see dashed lines in Fig. 2(a,b)).

### III. EXACT FIRING RATE MODEL

In the thermodynamic limit, Eqs. (1,2) with  $\Gamma = 0$  are exactly described by a low-dimensional system of differential equations that we refer to as QIF-FRM [21]. Inspired by recent results in the context of the Kuramoto model [36, 37], we next show that an identical set of exact FRM is obtained if, in addition to heterogeneity, neurons are driven by independent Cauchy noise [43].

#### A. Fractional Fokker-Planck equation and Lorentzian ansatz

Adopting the thermodynamic limit,  $N \rightarrow \infty$ , the macroscopic state of the QIF network is given by the probability density function of neurons having membrane potential  $V$  at time  $t$ ,

$$Q(V, t) = \int_{-\infty}^{\infty} P(V, t; \eta) G(\eta) d\eta, \quad (4)$$

where  $P(V, t; \eta)$  are conditional densities for specific values of  $\eta$ . In the thermodynamic limit,  $N \rightarrow \infty$ , the time evolution of the conditional densities  $P(V, t; \eta)$  is given by a Fractional Fokker-Planck Equation (FFPE) [44–46]. This equation involves the Riesz fractional derivative, which is usually defined in Fourier space (for an equivalent description that avoids the use of Riesz derivatives see Appendix A). We introduce the Fourier transform and its inverse as

$$\mathcal{F}\{f(V, t)\} = \int_{-\infty}^{\infty} f(V, t) e^{ikV} dV$$

and

$$\mathcal{F}^{-1}\{\tilde{f}(k, t)\} = \frac{1}{2\pi} \int_{-\infty}^{\infty} \tilde{f}(k, t) e^{-ikV} dk.$$

Then, the Riesz operator  $\frac{\partial^\alpha}{\partial|V|^\alpha} P(V, t)$  is defined as

$$\mathcal{F}\left\{\frac{\partial^\alpha f(V, t)}{\partial|V|^\alpha}\right\} = -|k|^\alpha \mathcal{F}\{f(V, t)\}. \quad (5)$$

For Cauchy noise we are only interested in the case  $\alpha = 1$ . With this definition, the FFPE for the time evolution of the densities  $P$  reads

$$\begin{aligned} \tau_m \frac{\partial P}{\partial t}(V, t; \eta) = & \quad (6) \\ - \frac{\partial}{\partial V} \{ [V^2 + \eta - \tau_m J s(t)] P(V, t; \eta) \} + \Gamma \frac{\partial P}{\partial|V|}(V, t; \eta). \end{aligned}$$

For  $\Gamma = 0$ , we recover the continuity equation for deterministic dynamics. This case was solved in [21] assuming that the conditional probabilities  $P$  are Cauchy distributions with width and center parameters that depend on  $t$  and  $\eta$ , namely  $x(t, \eta)$  and  $y(t, \eta)$ ,

$$P(V, t, \eta) = \frac{1}{\pi} \frac{x(t, \eta)}{[V - y(t, \eta)]^2 + x(t, \eta)^2}. \quad (7)$$

Here, we employ the same Lorentzian ansatz to solve the FFPE (6) for arbitrary  $\Gamma$ .

The Fourier transform of  $P$  reads  $\tilde{P}(k, t) = \exp\{iky - |k|x\}$ , thus,

$$\begin{aligned} \frac{\partial P}{\partial|V|}(V, t) &= \frac{-1}{2\pi} \int_{-\infty}^{\infty} |k| e^{-ik(V-y) - |k|x} dk \\ &= \frac{1}{\pi} \frac{(V-y)^2 - x^2}{[(V-y)^2 + x^2]^2}, \end{aligned} \quad (8)$$

where we have performed the integrals by parts. We replace this last expression (Eq. (8)) in the FFPE (6), and expand the partial derivatives using Eq. (7). After simplifying, we obtain a polynomial equation for  $V$ , which can be solved by equating the coefficients of like powers of  $V$  on both sides of the expression. As a result, we obtain two differential equations for the time evolution of  $x(t, \eta)$  and  $y(t, \eta)$ :

$$\begin{aligned} \tau_m \dot{x}(t, \eta) &= \Gamma + 2x(t, \eta)y(t, \eta) \\ \tau_m \dot{y}(t, \eta) &= \eta + y(t, \eta)^2 - x(t, \eta)^2 - J\tau_m s(t). \end{aligned}$$

In a homogeneous population of neurons ( $\Delta = 0$ ) these two equations would already provide a macroscopic description of the system. For a heterogeneous population with Cauchy-distributed heterogeneities ( $\Delta > 0$ ), a low-dimensional system can be attained by solving the integral in Eq. (4). In order to do so we define the complex variables  $w(t, \eta) := x(t, \eta) + iy(t, \eta)$ , thus

$$\tau_m \dot{w}(t, \eta) = i[\eta - w(t, \eta)^2 + J\tau_m s(t)] + \Gamma. \quad (9)$$

Considering the analytic continuation of  $w(t, \cdot)$  to the complex plane provides  $P(V, t; \cdot)$  as a holomorphic function. Therefore, we can compute the integral in Eq. (4) using Cauchy's residue theorem along the closed semicircle  $|\eta|e^{i\theta}$  with  $\theta \in (-\pi, 0)$  and  $|\eta| \rightarrow \infty$  [21]. As a result we obtain

$$Q(V, t) = P(V, t; \bar{\eta} - \Delta i). \quad (10)$$

### B. Mean membrane potential and mean firing rate

Equation (10) shows that  $Q$  is a Lorentzian distribution. Its center corresponds to the mean membrane potential of the QIF population, and thus we denote it as  $v(t) := y(t, \bar{\eta} - \Delta i)$  [47]. On the other hand, the mean firing rate of the neural population is given by

$$r(t) = \int_{-\infty}^{\infty} G(\eta) \tilde{r}(t, \eta) d\eta \quad (11)$$

where  $\tilde{r}(t, \eta)$  is the firing rate of the subset of neurons with current  $\eta$ . This quantity can be computed as the probability flux of the FFPE (6) at  $V \rightarrow \infty$ . The probability flux of (6) at a given point  $V$  is given by two terms: First, the flux given by the deterministic flow of the QIF dynamics,

$$\tau_m^{-1} [V^2 + \eta + \tau_m J s(t)] P(V, t; \eta).$$

Second, the total probability change rate provided by the stochastic dynamics in the interval  $(V, \infty)$ . Using Eq. (8) this can be computed as

$$\frac{\Gamma}{\pi \tau_m} \int_V^{\infty} \frac{(U - y)^2 - x^2}{[(U - y)^2 + x^2]^2} dU = \frac{\Gamma}{\pi \tau_m} \frac{V - y}{x^2 + (V - y)^2}.$$

Altogether, we have that

$$\tilde{r}(t, \eta) = \lim_{V \rightarrow \infty} \frac{1}{\tau_m} \left\{ [V^2 + \eta + \tau_m J s(t)] P(V, t; \eta) + \frac{\Gamma}{\pi \tau_m} \frac{V - y}{x^2 + (V - y)^2} \right\} = \frac{x(t, \eta)}{\tau_m \pi}.$$

Replacing this expression in Eq. (11) provides the firing rate of the entire QIF population as  $r(t) = x(t, \bar{\eta} - \Delta i) / (\pi \tau_m)$ .

Finally, replacing  $y = v$ ,  $x = \pi \tau_m r$ , and  $\eta = \bar{\eta} - \Delta i$  in Eq (9) and taking real and imaginary part leads to

$$\begin{aligned} \tau_m \dot{r} &= \frac{\Gamma + \Delta}{\pi \tau_m} + 2rv \\ \tau_m \dot{v} &= \bar{\eta} + v^2 - (\pi \tau_m r)^2 - J\tau_m s, \end{aligned} \quad (12)$$

which, together with Eq. (2), exactly describe the behavior of the QIF network Eqs. (1,2). Remarkably, Eqs. (12) illustrate that, in the thermodynamic limit, the level of heterogeneity  $\Delta$  and the level of noise  $\Gamma$  play identical roles at the collective level in populations of globally coupled QIF neurons.

### IV. THE QIF-FRM CAPTURES FAST OSCILLATIONS WITH LOW FIRING RATES

For the deterministic case,  $\Gamma = 0$ , the dynamics of Eqs. (12,2) have been analyzed in [18]. In the following we extend this analysis to networks of QIF neurons with both heterogeneity and noise.

Eqs. (12,2) have a single fixed-point corresponding to an asynchronous state. For small enough disorder  $\Delta + \Gamma$  and  $\tau_s, \bar{\eta} > 0$ , this steady state loses stability via a supercritical Hopf bifurcation, leading to the emergence of fast oscillations. The phase diagram Fig. 3 shows the Hopf boundaries for different values of  $\bar{\eta} > 0$  as a function of the strength of inhibition,  $J$ , and the level of disorder,  $\Delta + \Gamma$ . Oscillations occur for small enough values of the disorder, i.e. to the left of the Hopf boundaries.

To characterize neuronal activity within the region of oscillations, we compare the frequency of the collective rhythm  $\Omega$ , with the mean firing frequency of the individual neurons, given by the time-averaged mean firing rate  $\langle r \rangle$ . Notably, the ratio  $\langle r \rangle / \Omega$  (measuring the average spiking activity per oscillation cycle), is independent of whether the network is heterogeneous, stochastic, or both heterogeneous and stochastic —see the colored region in Fig. 3, which shows  $\langle r \rangle / \Omega$  for  $\bar{\eta} = 100$  computed from numerical simulations of the FRM (12,2).

For moderate disorder, Fig. 3 shows that the transition from asynchronous to synchronous activity occurs in two different ways depending on  $J$ . For small inhibition most neurons behave as self-sustained oscillators frequency entrained by the collective oscillation. This case corresponds to the yellow regions in Fig. 3, and to columns (a) and (b) of Fig. 1.

By contrast, for strong  $J$  suppression of firing dominates, and oscillations are only maintained by a few active neurons, see blue region in Fig. 3. In this case the population firing rate becomes considerably smaller than the oscillation frequency, see columns c and d of Figs 1. For the case of stochastic neurons, this corresponds to sparse synchronization.

The differences between the spiking behavior of neural networks prompted a distinction between sparse and 'regular' synchronization, which is often invoked in theoretical neuroscience [4–6, 10]. However, from the viewpoint of the mean field Eqs. (12,2), oscillations with high and low  $\langle r \rangle / \Omega$  correspond to the same periodic attractor, i.e., the transition between regular and irregular firing activity is smooth and does not involve any bifurcation. We illustrate this for stochastic networks in Figure 4. For both moderate  $J = 100$  (black symbols), and strong  $J = 400$  inhibition, noise gradually increases the difference between  $\Omega$  and  $\langle r \rangle$  (see panel a), as well as the firing irregularity monitored by the CV (see panel b). For moderate inhibition, neurons remain in a fairly regu-

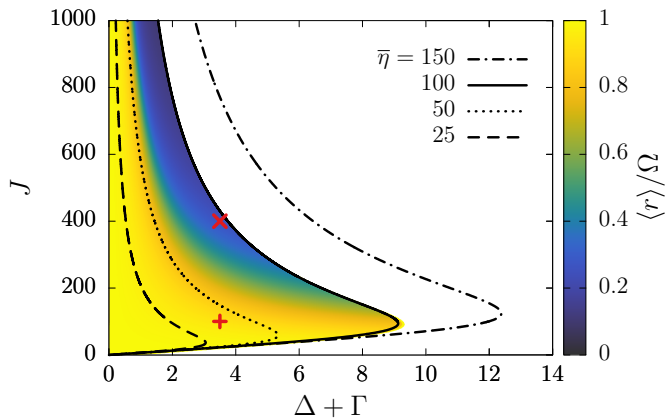


FIG. 3. Phase diagram of Eqs. (12,2). Black lines: Supercritical Hopf bifurcations for different values of  $\bar{\eta}$ , obtained using AUTO-07p [48]. The colormap corresponds to the average number of spikes per oscillation cycle for  $\bar{\eta} = 100$ , and numerically obtained computing  $\Omega$  and  $\langle r \rangle$  using the QIF-FRM, Eqs. (12,2). Symbol +: parameter values corresponding to Fig. 1 panels (a1)–(a3) and (b1)–(b3); Symbol  $\times$ : parameter values corresponding to Fig. 1 panels (c1)–(c3) and (d1)–(d3).

lar regime up to the Hopf bifurcation. Conversely, for strong inhibition the frequency difference and spike irregularities increase rapidly with  $\Gamma$ . If, instead, we fix the total amount of disorder and transition from a heterogeneous to a stochastic network, then  $\Omega$  and  $\langle r \rangle$  remain constant whereas the CV rapidly changes (see Appendix B 1).

The shape of the Hopf boundaries in Fig. 3 indicate that the oscillation region shrinks as coupling increases. This contrasts with setups using Gaussian noise [8, 10, 11], which show a persistence of the oscillatory dynamics for arbitrary strong inhibition and moderate disorder. In Appendix B 2 we show that this is also the case for populations of QIF neurons with Gaussian noise or heterogeneity (see also [33]). Therefore, though Cauchy noise appears to be more disruptive of the network synchronicity, we find that Gaussian and Cauchy distributions produce the same type of dynamical behaviors [49].

## V. CONCLUSIONS

Fast neural oscillations with irregular spike discharges at low firing rates—the sparse synchronization regime [6]—are pervasive in brain networks, and are successfully reproduced in numerical simulations of large spiking neuron networks with delayed inhibition and noise [8–11]. Yet, the extent to what FRM (that are powerful and broadly used tools for the analysis of neuronal dynamics) describe sparse synchrony remains elusive. Moreover, sparsely synchronized states are considered to be more robust and at odds with the non-sparse synchronized states emerging in deterministic populations of self-sustained oscillators [5, 6, 10].

Here we derived an exact FRM—Eqs. (12,2)—that unambiguously links fast global oscillations with the presence of sparse synchronization at the single-cell level. In addition, we

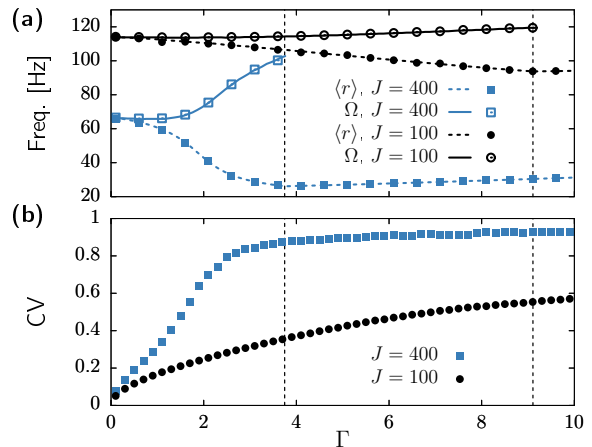


FIG. 4. (a) Oscillation frequency  $\Omega$  and time-averaged firing rate  $\langle r \rangle$  of a homogeneous network ( $\Delta = 0$ ) of QIF neurons vs. noise intensity  $\Gamma$ . Results obtained using Eqs. (1,2) (symbols) and Eqs. (12,2) (lines), for  $J = 100$  (black) and  $J = 400$  (blue). Vertical dashed lines indicate the location of the Hopf bifurcations for  $J = 100$  ( $\Gamma \simeq 9.11$ ) and for  $J = 400$  ( $\Gamma \simeq 3.75$ ). (b) Coefficient of variation (CV) of the ISI, obtained using the network Eqs. (1,2).

demonstrate that precisely the same FRM describes fast oscillations emerging in networks of deterministic, self-sustained oscillators. Therefore, our results indicate that only the neurophysiological mechanisms leading to the emergence of fast neuronal oscillations (inhibition, synaptic kinetics and/or delays and sufficient drive to induce spiking) determine the nature of the large-scale dynamics of the network, and not the level of regularity of the single neuron spiking activity. In [10] a similar equivalence between noise (Gaussian) and heterogeneity (uniform) was numerically observed. However, that analysis of networks with heterogeneity did not include the case of strong coupling, and the main focus was put on stochastic networks.

Altogether, our results reconcile two traditionally confronted views on the nature of fast neural rhythms (sparse vs. non-sparse synchronization) [5, 6, 10] and upgrades the applicability of exact FRM for QIF neurons to describe a broad range of biologically realistic neuronal states. Furthermore, our results can be readily extended to incorporate noise in a variety of extensions of the QIF-FRM, such as in interacting communities of excitatory and inhibitory populations [21], or in populations with conductance-based [23], or electrical synapses [26, 50, 51].

## ACKNOWLEDGMENTS

The authors thank Jordi Garcia-Ojalvo for helpful discussions. PC acknowledges financial support from the European Union’s Horizon 2020 research and innovation programme under grant agreement No 101017716 (Neurotwin). EM acknowledges support by the Agencia Estatal de Investigación under the Project No. PID2019-109918GB-I00.

## Appendix A: Cauchy noise as a limit of a Poisson process

Here we discuss a different interpretation of the Cauchy noise, which leads to a derivation of the mean-field theory that avoids the use of the Riesz operator. Let us assume now a more general case of Eq. (1) in which the random variables  $\xi_j(t)$  in Eq (1) correspond to a Poisson shot process with rate  $\nu$  and independent random increments given by a probability density  $F(u)$ . Then, the macroscopic equation for the time evolution of  $P$  is given by the Generalized Fokker-Planck Equation (GFPE) [37, 45, 46, 52]

$$\begin{aligned} \tau_m \frac{\partial P}{\partial t}(V, t; \eta) = & -\frac{\partial}{\partial V} \{ [V^2 + \eta - \tau_m J s(t)] P(V, t; \eta) \} \\ & + \nu \int_{-\infty}^{\infty} F(u) P(V - u, t; \eta) du - \nu P(V, t; \eta) . \end{aligned} \quad (\text{A1})$$

The right-hand-side of this integro-partial differential equation contains three terms. First, the advection term corresponding to the deterministic flow in Eq. (1). Second, a convolution integral accounting for the increase of probability due to the Poisson shot process with rate  $\nu$  and increments  $F(\cdot)$ . This can be interpreted as a *source* term in a continuity equation. And third, the loss of probability with rate  $\nu$  due to the stochastic dynamics, which can be interpreted as a *sink* term.

We consider  $F(\cdot)$  a Lorentzian distribution centered at zero and with half-width at half maximum  $\Gamma\nu^{-1}$ ,

$$F(u) := \frac{1}{\pi} \frac{\Gamma\nu}{(\nu u)^2 + \Gamma^2} .$$

In this case, the limit  $\nu \rightarrow \infty$  corresponds to  $\xi$  being the Cauchy white noise used in the main text. Indeed, in this limit, the GFPE (A1) corresponds to the FFPE (6), as we shall prove next.

Let us rewrite the GFPE (A1) as

$$\begin{aligned} \tau_m \frac{\partial P}{\partial t}(V, t; \eta) = & -\frac{\partial}{\partial V} \{ [V^2 + \eta + \tau_m J s(t)] P(V, t; \eta) \} \\ & + \nu [P * (F - \delta)](V) . \end{aligned}$$

where  $\delta$  is a Dirac delta function and  $*$  is the convolution operator

$$[f * g](x) = \int_{-\infty}^{\infty} f(y)g(x - y)dy .$$

Then, the Fourier transform of the stochastic term of the GFPE reads

$$\mathcal{F} \{ \nu [P * (F - \delta)](V) \} = \nu \tilde{P}(k, t) (\tilde{F}(k) - 1) .$$

where  $\tilde{P}(k, t) = \mathcal{F}\{P(V, t)\}$  and  $\tilde{F}(k) = \mathcal{F}\{F(V)\}$ . Since  $F$  is a Lorentzian,  $\tilde{F}(k) = \exp(-i|k|\Gamma\nu^{-1})$ . Therefore

$$\lim_{\nu \rightarrow \infty} \nu \tilde{P}(k, t) (\tilde{F}(k) - 1) = -\Gamma|k| \tilde{P}(k, t) ,$$

i.e., the integral term in the GFPE (A1) corresponds to the Riesz fractional derivative (5) with  $\alpha = 1$ .

To conclude, we show that our results still hold if the limit  $\nu \rightarrow \infty$  is taken after computing the integral term in the GFPE (A1). Using the ansatz (7), the integral on the right hand side of the GFPE (A1) corresponds to the convolution of two Lorentzian distributions. Since the sum of two Cauchy random variables also follows a Cauchy distribution (see, e.g., [53]), such convolution integral is readily solved as,

$$\int_{-\infty}^{\infty} F(u) P(V - u, t; \eta) du = \frac{1}{\pi} \frac{x + \Gamma\nu^{-1}}{(V - y)^2 + (x + \Gamma\nu^{-1})^2} .$$

Therefore

$$\begin{aligned} & \nu \int_{-\infty}^{\infty} F(u) P(V - u, t; \eta) du - \nu P(V, t; \eta) \\ & = \frac{\nu}{\pi} \left[ \frac{x + \Gamma\nu^{-1}}{(V - y)^2 + (x + \Gamma\nu^{-1})^2} - \frac{x}{(V - y)^2 + x^2} \right] \\ & \xrightarrow{\nu \rightarrow \infty} \frac{\Gamma}{\pi} \frac{(V - y)^2 - x^2}{[(V - y)^2 + x^2]^2} \end{aligned}$$

which coincides with the Riesz derivative of  $P$  given in Eq. (8) multiplied by the noise coefficient  $\Gamma$ .

## Appendix B: Supplementary numerical results

### 1. Combining heterogeneity and noise

Figure 4 of the main text shows how increasing noise in a network of QIF neurons smoothly transitions the system from a state in which the neurons fire regularly ( $CV \approx 0$ ) to a irregular microscopic activity ( $CV \approx 1$ ). Here we provide further evidence of the equivalence, at the collective level, of noise and heterogeneity, in spite of clear differences in the spiking regularity of single neurons.

We performed simulations of  $N = 8192$  described by Eq. (1) keeping the level of disorder constant at  $\Delta + \Gamma = 3.5$ , but varying the ratios of noise and heterogeneity. In order to do so we introduce a new parameter  $p \in [0, 1]$  quantifying the amount of heterogeneity in the network, i.e.,  $p = \Delta/(\Delta + \Gamma)$ .

The results are depicted in figure 5, which shows the collective frequency  $\Omega$  and the time-average mean firing rate  $\langle r \rangle$  (panel a); and the average coefficient of variation (CV, panel b). In order to compute the average CV, neurons with less than 2 spikes have been discarded from the computation (since at least 2 spikes are needed to obtain at least one ISI).

For  $p = 0$  we recover the case depicted in column (d) of Figure 1 of the main text, in which neurons fire irregularly, and thus  $CV \approx 1$ . As the amount of heterogeneity increases in the network, the regularity of the firing also increases, corresponding to a smooth decrease of the CV, which attains  $CV \approx 0$  for the full deterministic case ( $p = 1$ ). However, both, the macroscopic oscillatory frequency  $\Omega$  and the time-average mean firing rate  $\langle r \rangle$  remain unchanged by  $p$ , as can be inferred from the FRM (Eqs. (12,2)).

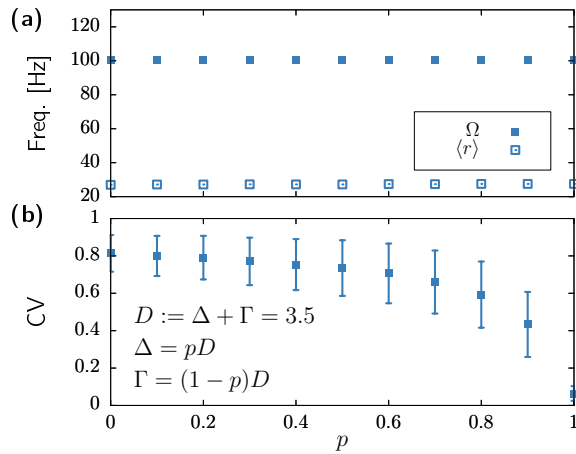


FIG. 5. Oscillation frequency  $\Omega$  and time-averaged firing rate  $\langle r \rangle$  of a network QIF neurons with fixed disorder  $\Gamma + \Delta = 3.5$  and varying the amount of heterogeneity  $p$ . Results obtained integrating Eqs. (12,2) of the main text for  $J = 400$  and the rest of the parameters set as in the main paper. (b) Average coefficient of variation (CV) of the ISI corresponding to the same simulations. Error bars indicate sample standard deviation.

## 2. Numerical results with Gaussian heterogeneity and noise

The remarkable analytical properties of Cauchy-Lorentz distributions allow one to derive exact mean-field equations for QIF neurons with such distributions of noise and heterogeneity. However, in simulations of spiking neurons it is usually more common to use Gaussian distributions due to their apt statistical properties. Unfortunately, to date, no exact low-dimensional reduction exists for QIF neurons with Gaussian heterogeneities or noise, although notable progress has been made in this direction. Next we discuss the case of Gaussian heterogeneity and Gaussian noise separately.

In [33] the authors proposed exact mean-field equations for networks of QIF neurons with  $q$ -Gaussian heterogeneities. Such distributions are indexed by a parameter  $n = 1, \dots, \infty$ ,

( $n = (q - 1)^{-1}$ ), for which  $n = 1$  corresponds to Lorentzian heterogeneity and Gaussian heterogeneity is achieved in the limit  $n \rightarrow \infty$ . The dimensionality of the resulting firing rate equations is  $2n$ , plus an additional equation for the synaptic dynamics Eq. (2). Therefore, a network with purely Gaussian heterogeneities remains described by an infinite-dimensional system.

In figure 6(a) we show a bifurcation diagram for QIF neurons with  $q$ -Gaussian heterogeneities for different values of  $n$ . We use the half-width at half-maximum (HWHM)  $d$  as control parameter of the heterogeneity. Notice that  $d = \Delta$  for a Cauchy distribution ( $n = 1$ ) and  $d = \sigma\sqrt{2\ln(2)}$  for a Gaussian distribution with standard deviation  $\sigma$  ( $n \rightarrow \infty$ ). Black line in figure 6 corresponds to the black continuous line in Fig. 3. As  $n$  increases, the region of oscillations widens. The colormap shows the level of activity in the region of oscillations obtained using simulations of Eqs. (1,2), but considering  $\eta_j$  to be distributed as a Gaussian with mean  $\bar{\eta}$  and standard deviation  $\sigma$ . In spite of the enlargement of the instability region, the Hopf bifurcation remains displaying two different cases: For low coupling  $J$  most neurons remain active even at the bifurcation line ( $\Omega \approx \langle r \rangle$ ). Instead, for high coupling there is a large degree of suppression as  $d$  increases.

For Gaussian noise, attempts to derive mean-field equations have been put forward [54–57]. However, these theories build on weak noise approximations ( $\sigma \ll 1$ ) and are thus unsuitable to analyze networks with large fluctuations. Figure 6(b) displays a numerical bifurcation diagram of the QIF network (Eqs. (1,2)) with  $\xi_i(t)$  being Gaussian white noise with standard deviation  $\sigma = d/\sqrt{2\ln(2)}$ . The scenario remains remarkably similar to the case of Gaussian heterogeneity, with still two qualitatively different transitions towards stationarity as  $d$  is increased. It is worth noting that we did not find cluster states. This contrasts with the results of [11], which analyze a similar setup with other integrate-and-fire models and find cluster instabilities for very low levels of Gaussian noise. A possible explanation might be the lack of a fixed delay and/or a rise synaptic time in our modelling setup.

- 
- [1] Marlene Bartos, Imre Vida, and Peter Jonas, “Synaptic mechanisms of synchronized gamma oscillations in inhibitory interneuron networks,” *Nature Reviews Neuroscience* **8**, 45–56 (2007).
- [2] Miles A. Whittington, Roger D. Traub, and John G. R. Jefferys, “Synchronized oscillations in interneuron networks driven by metabotropic glutamate receptor activation,” *Nature* **373**, 612–615 (1995).
- [3] M.A Whittington, R.D Traub, N Kopell, B Ermentrout, and E.H Buhl, “Inhibition-based rhythms: experimental and mathematical observations on network dynamics,” *International Journal of Psychophysiology* **38**, 315–336 (2000).
- [4] Xiao-Jing Wang, “Neurophysiological and computational principles of cortical rhythms in cognition,” *Physiological Reviews* **90**, 1195–1268 (2010).
- [5] György Buzsáki and Xiao-Jing Wang, “Mechanisms of gamma oscillations,” *Annual Review of Neuroscience* **35**, 203–225 (2012).
- [6] Nicolas Brunel and Vincent Hakim, “Sparsely synchronized neuronal oscillations,” *Chaos: An Interdisciplinary Journal of Nonlinear Science* **18**, 015113 (2008).
- [7] Christoph Börgers, *An introduction to modeling neuronal dynamics*, Vol. 66 (Springer, 2017).
- [8] Nicolas Brunel and Vincent Hakim, “Fast Global Oscillations in Networks of Integrate-and-Fire Neurons with Low Firing Rates,” *Neural Computation* **11**, 1621–1671 (1999).
- [9] Nicolas Brunel, “Dynamics of sparsely connected networks of excitatory and inhibitory spiking neurons,” *Journal of Computational Neuroscience* **8**, 183–208 (2000).
- [10] P H E Tiesinga and Jorge V José, “Robust gamma oscillations in networks of inhibitory hippocampal interneurons,” *Network: Computation in Neural Systems* **11**, 1–23 (2000).

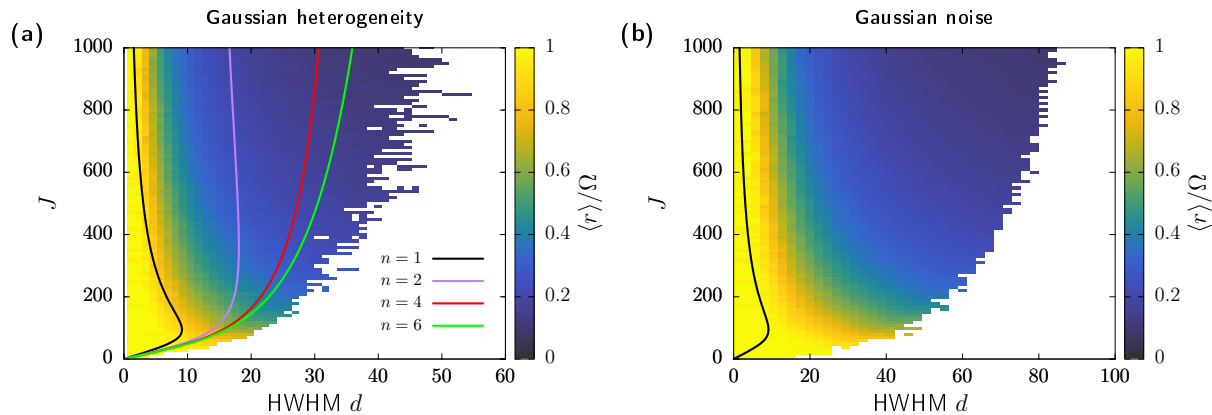


FIG. 6. Phase diagram of the QIF network with Gaussian distributions. (a) Lines: Supercritical Hopf bifurcations of the mean-field equations in [33] for different values of  $n$  (parameter values as in Fig. 3). The colormap corresponds to the average number of spikes per oscillation cycle for a QIF network with Gaussian heterogeneity. It has been numerically obtained through numerical integration of the QIF network Eqs. (12,2) of the main paper ( $N = 8192$ ). (b) Black line as in Fig. 3 of the main paper. Colormap corresponds to simulations of QIF neurons ( $N = 8192$ ) with Gaussian white noise and without heterogeneity (rest of the parameters as in the body of the paper). In both panels, a simulation has been considered to be in the oscillatory regime if the standard deviation of the synaptic activity  $s(t)$  is below  $10^{-3}$ .

- [11] Nicolas Brunel and David Hansel, “How Noise Affects the Synchronization Properties of Recurrent Networks of Inhibitory Neurons,” *Neural Computation* **18**, 1066–1110 (2006).
- [12] H. R. Wilson and J. D. Cowan, “Excitatory and inhibitory interactions in localized populations of model neurons,” *Biophysical journal* **12**, 1–24 (1972).
- [13] F. H. Lopes da Silva, A. Hoeks, H. Smits, and L. H. Zetterberg, “Model of brain rhythmic activity,” *Kybernetik* **15**, 27–37 (1974).
- [14] S. M. Ahn and Walter J. Freeman, “Steady-state and limit cycle activity of mass of neurons forming simple feedback loops (i): lumped circuit model,” *Kybernetik* **16**, 87–91 (1974).
- [15] Walter J. Freeman, *Mass Action in the Nervous System* (Elsevier, 1975).
- [16] A. Roxin, N. Brunel, and D. Hansel, “Role of delays in shaping spatiotemporal dynamics of neuronal activity in large networks,” *Phys. Rev. Lett.* **94**, 238103 (2005).
- [17] A. Roxin and E. Montbrío, “How effective delays shape oscillatory dynamics in neuronal networks,” *Physica D* **240**, 323–345 (2011).
- [18] Federico Devalle, Alex Roxin, and Ernest Montbrío, “Firing rate equations require a spike synchrony mechanism to correctly describe fast oscillations in inhibitory networks,” *PLoS Computational Biology* **13**, 1–21 (2017).
- [19] Federico Devalle, Ernest Montbrío, and Diego Pazó, “Dynamics of a large system of spiking neurons with synaptic delay,” *Phys. Rev. E* **98**, 042214 (2018).
- [20] Nicolas Brunel and Xiao-Jing Wang, “What determines the frequency of fast network oscillations with irregular neural discharges? i. synaptic dynamics and excitation-inhibition balance,” *Journal of Neurophysiology* **90**, 415–430 (2003), pMID: 12611969.
- [21] E. Montbrío, D. Pazó, and A. Roxin, “Macroscopic description for networks of spiking neurons,” *Phys. Rev. X* **5**, 021028 (2015).
- [22] Tanushree B. Luke, Ernest Barreto, and Paul So, “Complete Classification of the Macroscopic Behavior of a Heterogeneous Network of Theta Neurons,” *Neural Computation* **25**, 3207–3234 (2013).
- [23] Stephen Coombes and Áine Byrne, “Next generation neural mass models,” in *Nonlinear dynamics in computational neuroscience* (Springer, 2019) pp. 1–16.
- [24] Xiao-Jing Wang and György Buzsáki, “Gamma oscillation by synaptic inhibition in a hippocampal interneuronal network model,” *Journal of Neuroscience* **16**, 6402–6413 (1996).
- [25] John A White, Carson C Chow, Jason Rit, Cristina Soto-Treviño, and Nancy Kopell, “Synchronization and oscillatory dynamics in heterogeneous, mutually inhibited neurons,” *Journal of computational neuroscience* **5**, 5–16 (1998).
- [26] Carlo R. Laing, “Exact neural fields incorporating gap junctions,” *SIAM Journal on Applied Dynamical Systems* **14**, 1899–1929 (2015).
- [27] Diego Pazó and Ernest Montbrío, “From quasiperiodic partial synchronization to collective chaos in populations of inhibitory neurons with delay,” *Phys. Rev. Lett.* **116**, 238101 (2016).
- [28] Irmantas Ratas and Kestutis Pyragas, “Macroscopic oscillations of a quadratic integrate-and-fire neuron network with global distributed-delay coupling,” *Phys. Rev. E* **98**, 052224 (2018).
- [29] Hongjie Bi, Marco Segneri, Matteo di Volo, and Alessandro Torcini, “Coexistence of fast and slow gamma oscillations in one population of inhibitory spiking neurons,” *Phys. Rev. Research* **2**, 013042 (2020).
- [30] Marco Segneri, Hongjie Bi, Simona Olmi, and Alessandro Torcini, “Theta-nested gamma oscillations in next generation neural mass models,” *Frontiers in Computational Neuroscience* **14**, 47 (2020).
- [31] Andrea Ceni, Simona Olmi, Alessandro Torcini, and David Angulo-Garcia, “Cross frequency coupling in next generation inhibitory neural mass models,” *Chaos: An Interdisciplinary Journal of Nonlinear Science* **30**, 053121 (2020).
- [32] Stephen Keeley, Áine Byrne, André Fenton, and John Rinzel, “Firing rate models for gamma oscillations,” *Journal of Neurophysiology* **121**, 2181–2190 (2019).
- [33] Viktoras Pyragas and Kestutis Pyragas, “Mean-field equations for neural populations with  $q$ -gaussian heterogeneities,” *Phys. Rev. E* **105**, 044402 (2022).
- [34] Pau Clusella, Elif Köksal-Ersöz, Jordi Garcia-Ojalvo, and Giulio Ruffini, “Comparison between an exact and a heuristic

- neural mass model with second-order synapses,” *Biological Cybernetics* (2022), 10.1007/s00422-022-00952-7.
- [35] Viktoras Pyragas and Kestutis Pyragas, “Effect of Cauchy noise on a network of quadratic integrate-and-fire neurons with non-Cauchy heterogeneities,” *Physics Letters A* **480**, 128972 (2023).
- [36] Takuma Tanaka, “Low-dimensional dynamics of phase oscillators driven by cauchy noise,” *Phys. Rev. E* **102**, 042220 (2020).
- [37] Ralf Tönjes and Arkady Pikovsky, “Low-dimensional description for ensembles of identical phase oscillators subject to cauchy noise,” *Phys. Rev. E* **102**, 052315 (2020).
- [38] B. Ermentrout and N. Kopell, “Parabolic bursting in an excitable system coupled with a slow oscillation,” *SIAM J. Appl. Math.* **46**, 233–253 (1986).
- [39] E. M. Izhikevich, *Dynamical Systems in Neuroscience* (The MIT Press, Cambridge, Massachusetts, 2007).
- [40] The mean firing rate in Eq. (3) exactly corresponds to the firing rate variable described by Eqs. (12) if one first adopts the limit  $N \rightarrow \infty$ , and then  $\tau_r \rightarrow 0$ , see [21].
- [41] In numerical simulations of Eqs. (1,2), we used the Euler-Maruyama scheme with  $\delta t = 10^{-3}$ . Thus, at each time step, the random increments follow Cauchy distribution with HWHM  $dt\Gamma$ . In addition, we set  $V_p = -V_r = 100$ ,  $\bar{\eta} = 100$  and  $N = 8192$ . For heterogeneous networks,  $\eta_j$  are generated as  $\eta_j = \Delta \tan(\frac{\pi(2j-N-1)}{2(N+1)})$ , with  $j = 1, \dots, N$ . The mean firing rate  $r$  is computed using Eq. (3) with  $\tau_r = 10^{-2}$ . The time series of Fig 1(a1–d1) use an additional binning window of 0.1ms for display.
- [42] The coefficient of variation (CV) of the ISI provides a common measure of firing regularity. It is close to 0 for a delta distribution, close to 1 for Poisson spike times, and larger for even more irregular patterns.
- [43] See Ref. [58] for an alternative derivation. Additionally, see also recent attempts to obtain *approximated* mean field descriptions of populations of QIF neurons with independent Gaussian noise [54–57].
- [44] Ralf Metzler and Joseph Klafter, “The random walk’s guide to anomalous diffusion: A fractional dynamics approach,” *Physics Reports* **339**, 1–77 (2000).
- [45] J. Klafter and I. M. Sokolov, *First Steps in Random Walks: From Tools to Applications* (Oxford University Press, 2011).
- [46] Vicenç Méndez, Daniel Campos, and Frederic Bartumeus, *Stochastic Foundations in Movement Ecology* (Springer Berlin Heidelberg, 2014).
- [47] Notice that Lorentzian distributions do not have a well defined mean, thus  $v$  actually corresponds to the Cauchy principal value of the integral  $\int_{-\infty}^{\infty} Q(V, t)VdV$ .
- [48] Eusebius J Doedel, Alan R Champneys, Fabio Dercole, Thomas F Fairgrieve, Yu A Kuznetsov, B Oldeman, RC Paffenroth, B Sandstede, XJ Wang, and CH Zhang, “Auto-07p: Continuation and bifurcation software for ordinary differential equations,” (2007).
- [49] There exist no exact low-dimensional reductions for populations of QIF neurons with Gaussian disorder, and the approximated techniques proposed so far rely on weak noise assumptions [54–57].
- [50] Bastian Pietras, Federico Devalle, Alex Roxin, Andreas Daffertshofer, and Ernest Montbrió, “Exact firing rate model reveals the differential effects of chemical versus electrical synapses in spiking networks,” *Phys. Rev. E* **100**, 042412 (2019).
- [51] Ernest Montbrió and Diego Pazó, “Exact mean-field theory explains the dual role of electrical synapses in collective synchronization,” *Phys. Rev. Lett.* **125**, 248101 (2020).
- [52] S. I. Denisov, Werner Horsthemke, and Peter Hänggi, “Steady-state Lévy flights in a confined domain,” *Physical Review E* **77**, 061112 (2008).
- [53] Norman L Johnson, Samuel Kotz, and N Balakrishnan, *Continuous Univariate Distributions, Volume 1*, 2nd ed., Wiley Series in Probability and Statistics (John Wiley & Sons, Nashville, TN, 1994).
- [54] Denis S. Goldobin, Matteo di Volo, and Alessandro Torcini, “Reduction methodology for fluctuation driven population dynamics,” *Phys. Rev. Lett.* **127**, 038301 (2021).
- [55] Irmantas Ratas and Kestutis Pyragas, “Noise-induced macroscopic oscillations in a network of synaptically coupled quadratic integrate-and-fire neurons,” *Phys. Rev. E* **100**, 052211 (2019).
- [56] Denis S. Goldobin, “Mean-field models of populations of quadratic integrate-and-fire neurons with noise on the basis of the circular cumulant approach,” *Chaos: An Interdisciplinary Journal of Nonlinear Science* **31**, 083112 (2021).
- [57] Matteo di Volo, Marco Segneri, Denis S. Goldobin, Antonio Politi, and Alessandro Torcini, “Coherent oscillations in balanced neural networks driven by endogenous fluctuations,” *Chaos: An Interdisciplinary Journal of Nonlinear Science* **32**, 023120 (2022).
- [58] Bastian Pietras, Rok Cestnik, and Arkady Pikovsky, “Exact finite-dimensional description for networks of globally coupled spiking neurons,” *Phys. Rev. E* **107**, 024315 (2023).